ACS OMEGA

Open Access

http://pubs.acs.org/journal/acsodf

Article

Mechanisms of Ellagic Acid (EA)-Mediated Osteogenic Differentiation of Human Dental Pulp-Derived Stem Cells

Prathyusha Naidu, Manjusri Das, Surajit Hansda, Prateeksha Prateeksha, Md Sariful Islam Howlader, Md Afjalus Siraj, and Hiranmoy Das*

Cite This: *ACS Omega* 2025, 10, 15229−15242

Read Online

ACCESS | Metrics & More | Article Recommendations | Supporting Information

ABSTRACT: Ellagic acid (EA) is a potent antioxidant that reduces oxidative stress and promotes differentiation. By lowering the harmful levels of reactive oxygen species (ROS), EA fosters an environment conducive to the osteoblastic differentiation (OB) of stem cells. In addition, it promotes autophagy and mitophagy, which are vital for promoting differentiation. Effective autophagic activity recycles damaged organelles and proteins, meeting the energy required during differentiation and shielding from apoptosis. However, molecular mechanisms underlying the osteogenic differentiation of mesenchymal stem cells remain inadequately explored. Therefore, the current study aims to define the regulatory role of EA during the OB of dental pulp-derived stem cells (DPSC) and to study how autophagy and mitophagy are being modulated during this differentiation process. Herein, we showed that the expression level of osteoblast-specific markers, autophagy, and mitophagy-associated markers was significantly elevated during EA-mediated OB differentiation of DPSC. Moreover, we found that the EA induced the osteoblastic-specific markers through canonical BMP2 pathway molecules, reduced ROS in both basal and activated states, and induced autophagy and mitophagy molecules along with enhanced mitochondrial functions. Cell cycle analysis revealed that the G1 phase was arrested via phosphorylation of γ-H2AX, ATM, and CHK2 proteins. Furthermore, in silico analysis revealed that EA strongly binds with osteonectin, a crucial noncollagen protein involved in bone remodeling, and confirmed by Western blot analysis. These results support that EA could be a promising natural compound for bone repair and regeneration applications.

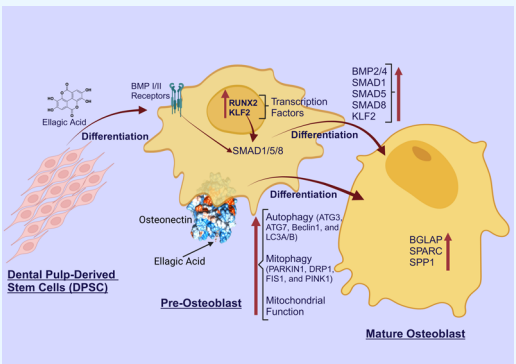

INTRODUCTION

Ellagic acid (EA) is a flavonoid polyphenolic compound with considerable antioxidant and anti-inflammatory effects. Fruits, such as pomegranates, pecans, and raspberries, contain a significant amount of EA with biologically and pharmacologically active flavonoid polyphenols.[1] This compound offers various physiological benefits, including antioxidant, anti-inflammatory, and antibacterial.[2] It also has the potential to be an anticancer agent because of its targeted mechanisms affecting cell growth, programmed cell death, DNA structure, and neovascularization.[1] The effect of EA on RANKL (receptor activator of nuclear factor kappa-β ligand)-induced osteoclast differentiation was also explored and showed that EA alleviates osteoclastogenesis by suppressing the p38 signaling pathway downstream of RANKL through bone remodeling.[2,3] It was also shown that EA-HA (hydroxyapatite) can increase osteogenesis in bone defects by increasing the number of osteoblasts and the expression of osteoprotegerin (OPG) and osteocalcin (OCN).[4] However, further investigation is required to understand the involvement of EA during the osteogenesis process. Therefore, using this EA to stimulate dental pulp-derived stem cells (DPSC) could be of interest to bone regeneration and to the maintenance of healthy bone conditions.

To develop treatment for any bone disease, it is crucial to have a clear understanding of the molecular and cellular mechanisms involved in bone physiology and pathology.[5] In healthy conditions, the bone remodels by the balanced activity of osteoclasts (OC), and osteoblasts (OB), through secreting organic and mineral components.[6−8] Structural deteriorations occur in the bones due to excessive resorption by osteoclasts and insufficient activity of osteoblasts to restore bone properly, resulting in osteoporosis.[6] Bone possesses a distinct quality unlike many other tissues and regenerates completely instead of healing with a scar after injury.[9] After the initial inflammatory phase, mesenchymal stem cells (MSC) and blood vessels are activated at the injury site and then start to regenerate into osteoblasts or chondrocytes.[10]

Received: December 4, 2024
Revised: March 5, 2025
Accepted: March 11, 2025
Published: April 13, 2025

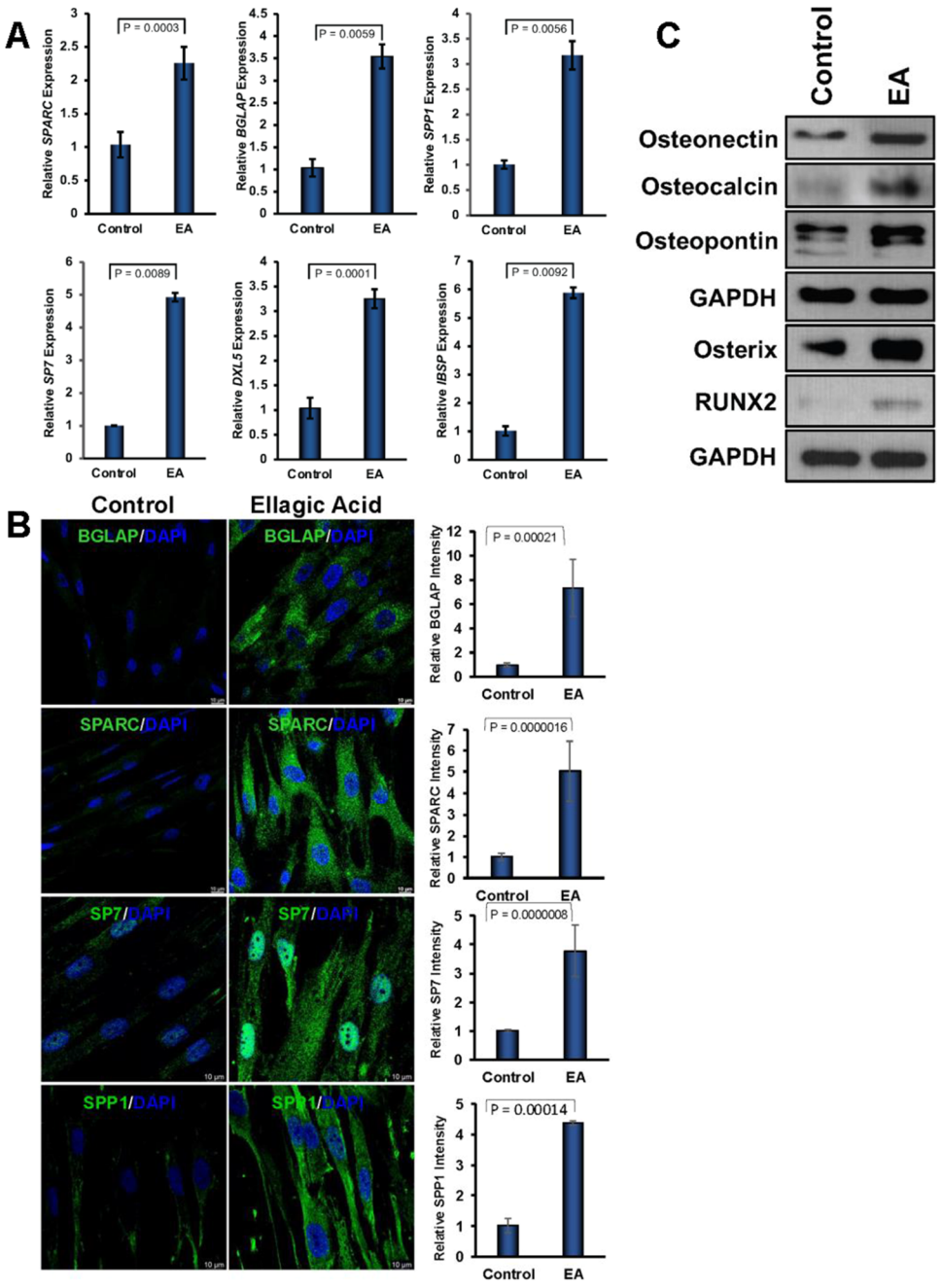

Figure 1. Ellagic acid (EA) induced marker molecules of osteoblast differentiation both in gene and protein levels. (A) The expression level of osteoblast differentiation markers shown graphically was determined by RT-qPCR after 7 days of DPSC in the presence or absence of EA (5 μM). (B) Confocal microscopy images were shown for osteogenic markers after 7 days of DPSC in the presence or absence of EA (5 μM). (C) Images of Western blot of osteogenic markers were shown after 7 days of DPSC in the presence or absence of EA (5 μM).

The exploration of MSC's significant clinical potential for bone healing for the treatment of bone disorders is being investigated. MSC, whether isolated and delivered for a therapeutic effect, or activated using biological or pharmacological means, shows great potential clinical promise.[10] DPSC are similar to MSC in nature isolated from dental pulp that possess the ability to self-renewal and regenerate tissues except have the potential to differentiate into neural cells.[11,12] They are known for their multipotential capacity, making them a promising tool for bone tissue regeneration.[6] DPSC exhibit a greater cell proliferation ability when compared to other types of stem cells.[13] Studies have shown that DPSC have great potential for bone tissue engineering,[14] whereas the addition of bone morphogenetic protein (BMP)-2 and growth factors on diverse polymeric and biological scaffolds have improved osteogenic differentiation of DPSC.[6]

BMPs are vital growth factors and belong to the transforming growth factor-β (TGF-β) superfamily. They play crucial roles in various developmental processes of neurogenesis, cardiogenesis, and osteogenesis.[15] BMP2 is the first BMP studied extensively and is essential in embryonic development, bone remodeling, and homeostasis during adulthood.[15,16] It also plays a role in promoting osteoblast differentiation and increasing the production of bone matrix by osteoblastic cells[17] and has been identified as a potential agent for promoting bone formation for the healing of fractures.[18]

https://doi.org/10.1021/acsomega.4c10642
ACS Omega 2025, 10, 15229−15242

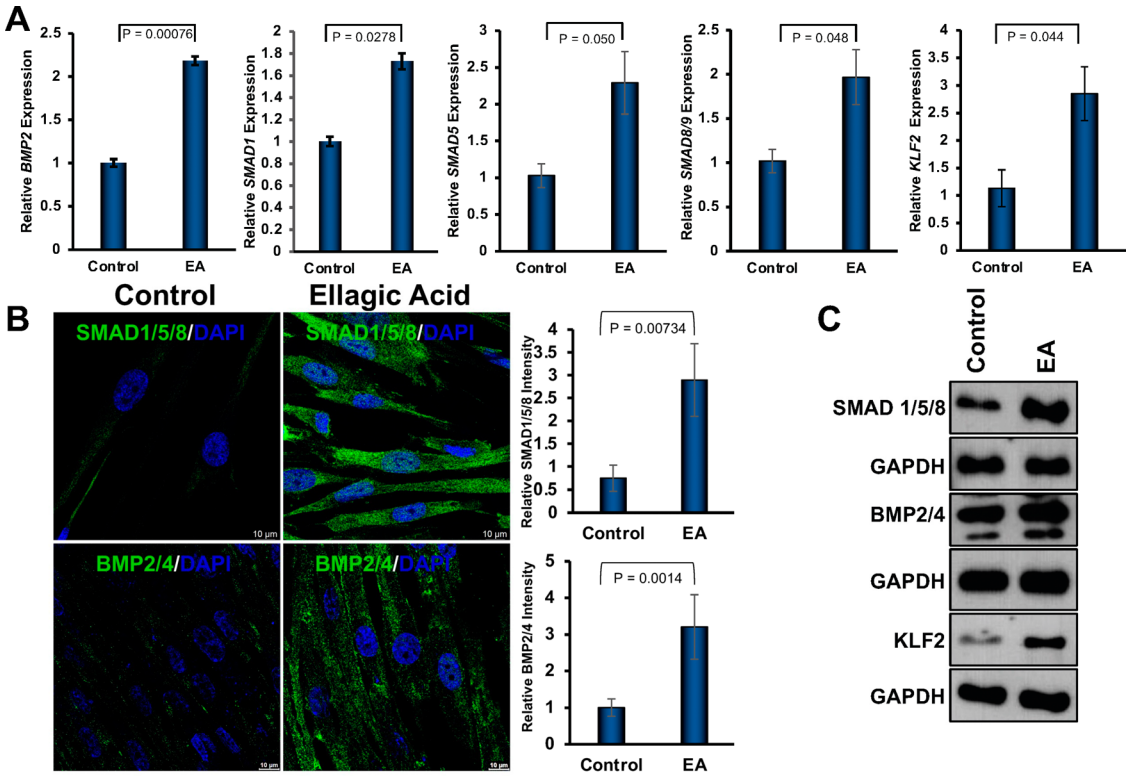

Figure 2. Ellagic acid-induced osteoblast differentiation pathway molecules both in gene and protein levels. (A) RT-qPCR evaluation of BMP2 signaling-associated markers in DPSC in the presence or absence of EA (5 μM) was shown graphically. (B) Confocal microscopy images were shown for BMP2 signaling markers after 7 days of DPSC in the presence or absence of EA (5 μM). (C) Images of a Western blot of BMP2 signaling markers and KLF2 were shown after 7 days of DPSC in the presence or absence of EA (5 μM).

SMAD 1/5/8 proteins play a crucial role in osteoblast differentiation by serving as important signaling molecules in the BMP pathway. Activated by BMPs, these SMADs move to the nucleus and control the expression of genes such as RUNX2, SP7, and DLX5, which are essential for osteoblast development. This, in turn, drives the differentiation of osteoblasts from progenitors.[19]

Several cellular functions and molecular signaling pathways regulate the coupling of osteoblasts and osteoclasts. Recently, autophagy has emerged as an integral part of the bone remodeling and regeneration process.[5] Autophagy is a complex dynamic system that plays a crucial role in maintaining cell homeostasis. Autophagy degrades and repairs intracellular proteins and organelles by maintaining the metabolism of bone tissue, particularly in response to various physiological or pathological conditions.[5] Studies have found that autophagy is essential for maintaining the homeostasis of bone marrow MSC-derived cells.[5]

Osteoporosis is closely associated with the enhanced level of inflammation, specifically with the enhancement of a nucleotide-binding domain leucine-rich repeat (NLR) family pyrin domain containing 3 (NLRP3) inflammasome that triggers the production of inflammatory cytokines through the activation of nuclear factor kappa-light-chain-enhancer of activated B (NF-κB) pathway molecules.[20,21] As a result, activation of NLRP3 and the NF-κB pathway hinders osteogenesis while promoting adipogenesis.[20,22] Medications for osteoporosis either block bone resorption or stimulate bone formation. However, their long-term usage can lead to several complications including hindering bone growth, causing gastrointestinal and hormonal issues, and muscular soreness.[21,23] They may even cause the pathogenesis of developing osteosarcoma. Treatment options like bisphosphonates and hormonal replacement therapies (HRT) are the most common therapeutics for osteoporosis.[21,24] These therapeutics prevent only further bone loss and cannot repair lost bone mineral density. Hence, it is crucial to develop a safer alternative therapy using natural compounds.[20,21,23]

This study aims to investigate the ability of EA to promote osteogenesis of human DPSC and define the involved in-depth mechanisms for the future development of stem cell therapy for bone regeneration.

RESULTS

Effect of EA in Promoting Osteogenic Differentiation of DPSC. DPSC were collected and evaluated for their properties using flow cytometry following earlier published protocols (data not shown).[6,25,26] To investigate whether EA shows the ability to differentiate DPSC into osteogenic lineages, we examined the expression of osteoblast-specific marker molecules like SPARC, BGLAP, SPP1, SP7, DXL5, and IBSP after the addition of EA (5 μM) to the DPSC for 7 days, and using RT-qPCR analysis and immunocytochemical staining. The RT-qPCR results showed that the mRNA expression of osteogenic markers was significantly increased after the addition of EA (Figure 1A). In addition, immunocytochemical staining results showed that the expression of investigated osteoblastic-specific markers BGLAP, SPARC, SP7, and SPP1 was significantly upregulated after the addition of EA (Figure 1B). We further confirmed the ability of EA to induce OB differentiation of DPSC using Western blotting analysis, and revealed that the investigated

https://doi.org/10.1021/acsomega.4c10642
ACS Omega 2025, 10, 15229−15242

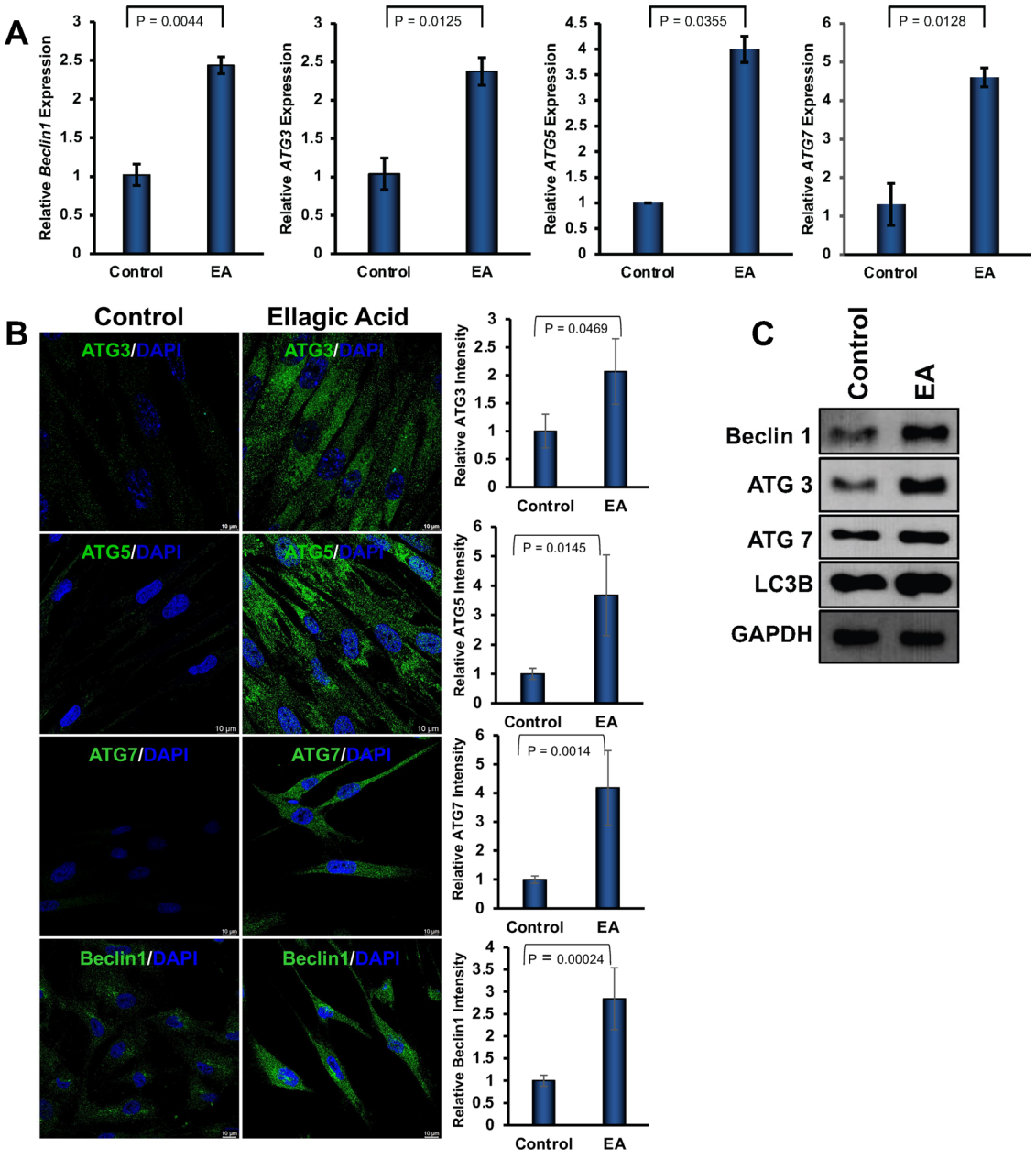

Figure 3. Ellagic acid-induced autophagic molecules both in gene and protein levels during osteoblastic differentiation. (A) RT-qPCR evaluation of autophagy-associated markers shown graphically after 7 days of DPSC in the presence or absence of EA (5 μM). (B) Confocal microscopy images were shown for autophagy markers after 7 days of DPSC in the presence or absence of EA (5 μM). (C) Images of Western blot of autophagy markers were shown after 7 days of DPSC in the presence or absence of EA (5 μM).

osteoblast-specific genes SPARC, BGLAP, SPP1, SP7, and RUNX2, were markedly increased after the addition of EA (Figure 1C). These results indicate that all the tested OB differentiation-specific genes were significantly elevated upon addition of EA at various degrees indicating that EA successfully induced DPSCs for OB differentiation.

Evaluation of EA-Induced Signaling Molecules. To gain a deeper understanding of the possible signaling molecules involved in an EA-induced OB differentiation of DPSCs, we examined markers specific to the BMP2 pathway such as BMP2/4, SMAD1, SMAD5, and SMAD8/9 genes. RT-qPCR analysis revealed that the gene levels of the tested molecules were increased significantly after the addition of EA to the DPSC (Figure 2A). Moreover, BMP2/4 and SMAD1/5/8 were also significantly increased after the addition of EA to the DPSC in the immunocytochemical staining. (Figure 2B). Western blot analysis revealed the expression of BMP2/4 and SMAD1/5/8 was increased after the addition of EA to the DPSC (Figure 2C). These results indicate that the EA induced the canonical BMP2 signaling pathway molecules.

Apart from this, we wanted to study the involvement of a well-known transcription factor, KLF2 associated with cellular differentiation[27−30] after the addition of EA to the DPSC. We found that both gene and protein levels of KLF2 were significantly increased after the addition of EA to the DPSC (Figure 2A,2C). These results indicate a possible involvement of KLF2 in EA-induced OB differentiation, which is under investigation and outside of the scope of this manuscript.

Effect on Autophagy after the Addition of EA to the DPSC. We further studied the involvement of autophagy

https://doi.org/10.1021/acsomega.4c10642
ACS Omega 2025, 10, 15229−15242

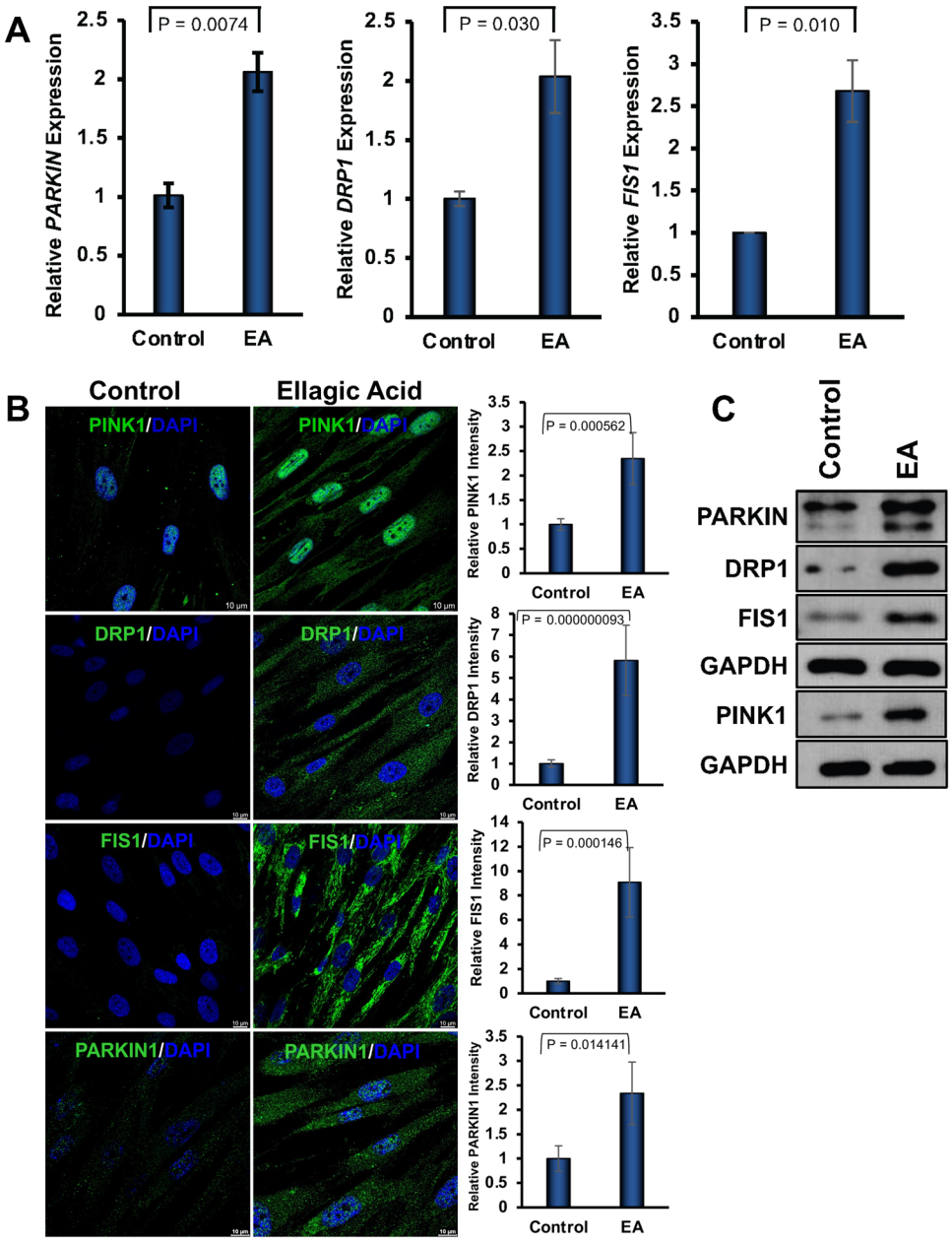

Figure 4. Ellagic acid-induced mitophagy molecules both in gene and protein levels during osteoblastic differentiation. (A) RT-qPCR evaluation of mitophagy-associated markers shown graphically after 7 days of DPSC in the presence or absence of EA (5 μM). (B) Confocal microscopy images were shown for mitophagy markers after 7 days of DPSC in the presence or absence of EA (5 μM). (C) Images of Western blot of mitophagy markers were shown after 7 days of DPSC in the presence or absence of EA (5 μM).

during the EA-induced osteogenic differentiation. The levels of autophagy molecules in the gene (determined by RT-qPCR) and protein levels (determined by immunofluorescence method) such as BECN1, ATG3, ATG5, and ATG7 were significantly increased after the addition of EA to the DPSC (Figure 3A,B). We further confirmed the level of autophagy molecules using the WB method. The results showed that the expression of BECN1, ATG3, ATG7, and LC3B molecules was significantly increased after the addition of EA to the DPSC (Figure 3C). These results suggest the involvement of autophagy in EA-induced OB differentiation.

Effect on Mitophagy after the Addition of EA to the DPSC. Further evaluation of mitochondrial dynamics markers revealed a significant upregulation of Parkin, DRP1, and FIS1 molecules at the gene level after the addition of EA to the DPSC (Figure 4A). In addition, similar trends were observed in protein expression of PINK1, DRP1, FIS1, and Parkin molecules determined by immunofluorescence methods (Figure 4B). Identical to the immunocytochemical results, we also found that the level of Parkin, DRP1, FIS1 and PINK1 was enhanced after the addition of EA to the DPSC determined by WB method (Figure 4C). These results suggest that the involvement of mitophagy in EA-induced OB differentiation.

Effect of EA on Intracellular and Mitochondrial ROS during EA-Induced OB Differentiation. As reactive oxygen species (ROS) acts as a stimulator for the various cell signaling pathways,[31,32] we next investigated the intracellular ROS generation and mitochondrial superoxide generation by DCFDA and MitoSOX staining respectively after the addition

https://doi.org/10.1021/acsomega.4c10642
ACS Omega 2025, 10, 15229−15242

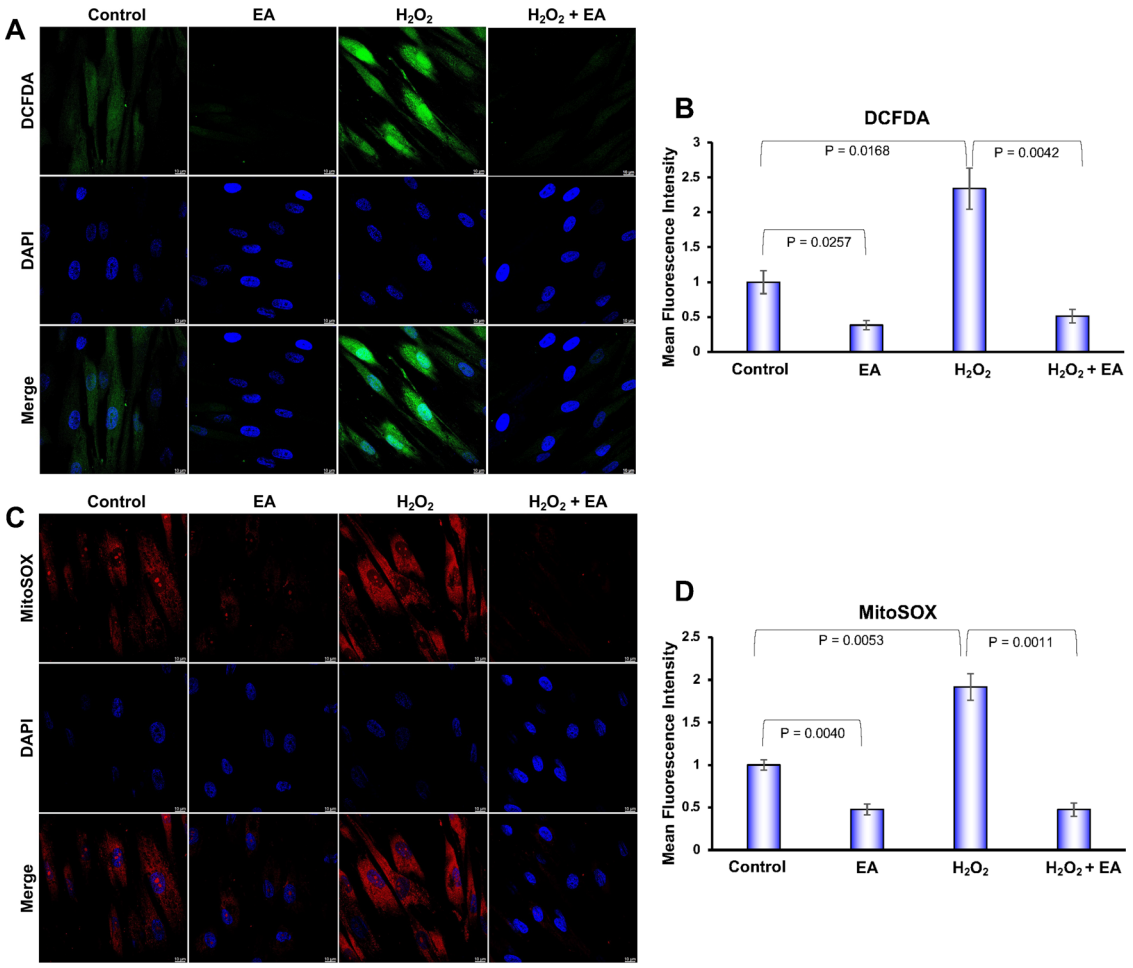

Figure 5. Ellagic acid reduced intracellular and mitochondrial ROS during osteoblastic differentiation. (A) Immunofluorescence images of intracellular ROS after 7 days of DPSC in the presence or absence of EA (5 μM) detected by DCFDA staining in basal and activated (H_2O_2) conditions. (B) Relative mean fluorescence intensity of the images shown graphically. (C) Immunofluorescence images of mitochondrial ROS after 7 days of DPSC in the presence or absence of EA (5 μM) detected by mitoSOX staining in basal and activated (H_2O_2) conditions. (D) Relative mean fluorescence intensity of the images shown graphically.

of EA to the DPSC. We found that EA-induced differentiated cells showed a significant decrease in ROS and mitochondria superoxide production both in the basal and activated (after the addition of H_2O_2, which induces intracellular ROS production) conditions compared to the control DPSC (Figure 5A–D).

Effect of EA on Mitochondrial Membrane Potential and Mitochondrial Function during EA-Induced OB Differentiation. An electrochemical proton gradient produced by the mitochondrial membrane drives the production of ATP.[33] Cations are drawn in while anions are drawn out due to the negative charge inside the mitochondria. To assess the potential of the mitochondrial membrane after the addition of EA to the DPSC, we stained DPSC with JC1 dye, which is a lipophilic cationic dye that produces green fluorescence naturally. JC1 dye forms reversible J aggregate complexes that produce red fluorescence when it is taken up by mitochondria. Healthy mitochondrial membrane potential results in red-stained spots, while cells with decreased membrane potential exhibit mostly green fluorescence. Our study showed that untreated DPSCs stained with JC1 dye had red-stained spots throughout the cytoplasm (Figure 6A,B). After the addition of EA to the DPSC, fewer, red-stained spots were observed in DPSC compared to the untreated control. Furthermore, we studied whether EA can alter the MMP in activated conditions by stimulating with carbonyl cyanide chlorophenylhydrazone (CCCP), which disrupts ATP synthesis by transporting protons across the mitochondrial inner membrane that can depolarize the plasma membrane and reduce ATP production. We found that the expression of red aggregates was significantly reduced in DPSC after the addition of EA compared to the without EA control (Figure 6A,B). This result suggests that there may be a reduction in mitochondrial membrane potential in DPSC after the addition of EA.

We next sought to examine the extracellular acidification rate defining the glycolytic metabolism in DPSC after the addition of EA. Significant increases were observed in the capacity for glycolysis, glycolytic reserve, nonglycolytic acidification, and glycolysis in differentiated cells (Figure 6C). To fulfill the energy demand in the absence of glutamine DPSC after differentiation catabolizes the glucose through the glycolysis pathway in a higher rate. We further examined the mitochondrial functions in the context of mitochondrial oxygen consumption rate (OCR) at basal respiration, mitochondrial respiration, spare respiration capacity, and ATP production in DPSC after the addition of EA. There is an increased level in both basal respiration and ATP production in DPSC after the addition of EA when compared

https://doi.org/10.1021/acsomega.4c10642
ACS Omega 2025, 10, 15229−15242

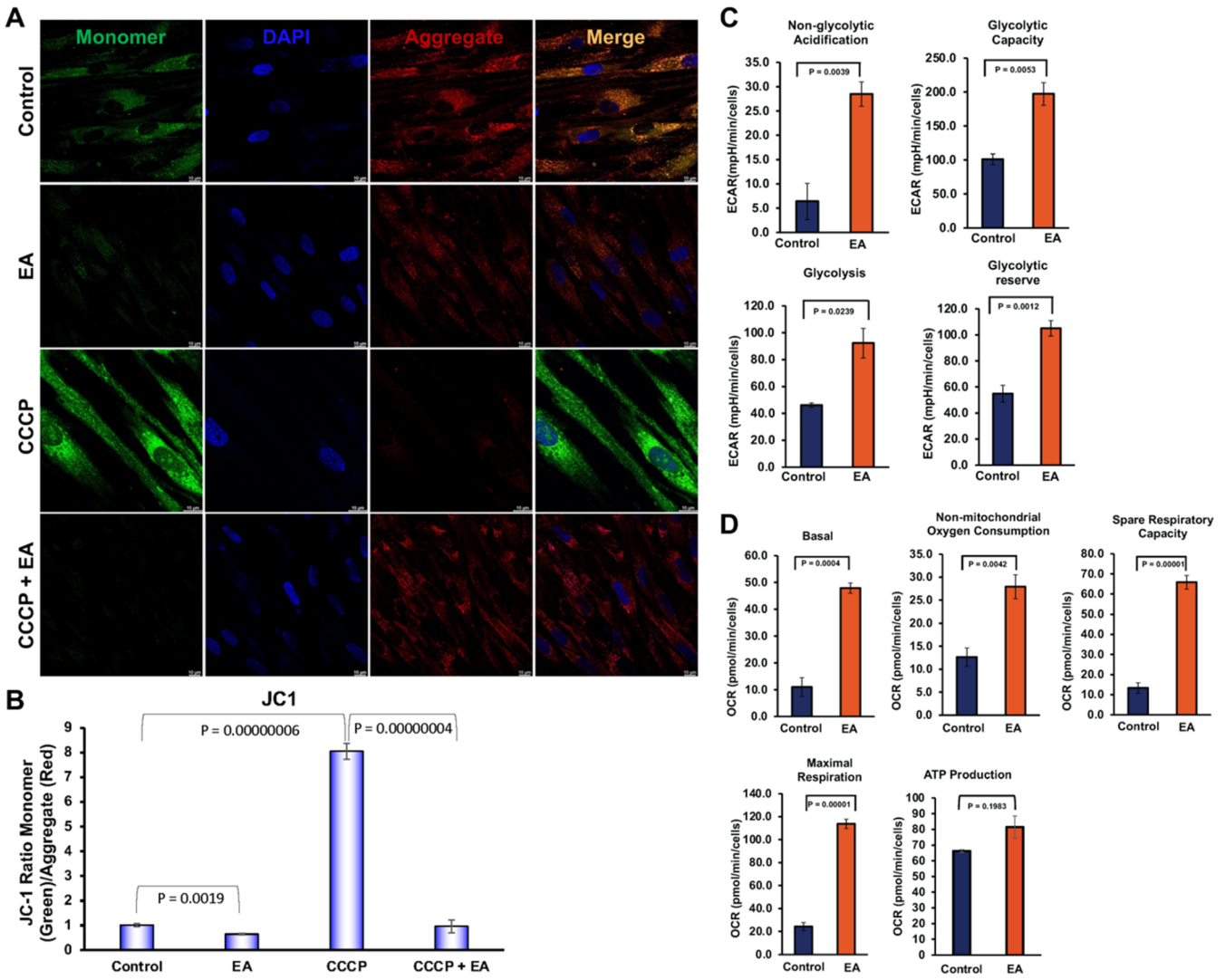

Figure 6. Ellagic acid-induced mitochondrial membrane potential and function during osteoblastic differentiation. (A) Immunofluorescence images of mitochondrial membrane potential after 7 days of DPSC in the presence or absence of EA (5 μM) detected by JC1 staining in basal and activated (carbonyl cyanide *m*-chlorophenylhydrazone, CCCP) conditions. (B) Relative mean fluorescence intensity of the images shown graphically. (C) Seahorse flux analysis of extracellular acidification rate (ECAR) in DPSC in the presence or absence of EA (5 μM) for 7 days. (D) Seahorse flux analysis of oxygen consumption rate (OCR) in DPSC in the presence or absence of EA (5 μM) for 7 days.

to the control group. This trend was also observed with the other parameters examined, including spare respiratory capacity, and maximal and mitochondrial respiration upon stimulation with EA (Figure 6D).

Effect of EA on Cell Cycle and Check-Point Molecules During EA-Induced OB Differentiation. We aimed to analyze the regulation of DPSC during OB differentiation throughout the cell cycle progression by flow cytometry in (Figure 7A). In control cells, 81.77%, of the cell population was in the G1 phase of the cycle. After the addition of EA to the DPSC for 7 days, a significant increase was observed in the percentage of cell population in the G1 phase (up to 86.6%) (Figure 7B). We found that after the addition of the EA to the DPSC the G1 phase of the cell cycle was arrested.

We further investigated to dissect which check-point protein was involved in arresting the G1 phase of the cell cycle. After WB analysis we found that γ-H2AX, ATM, and CHK2 were activated via phosphorylation in DPSC after the addition of the EA (Figure 7C).

In Silico Modeling for Binding between EA and Osteonectin. We conducted an in silico molecular interaction analysis to understand how EA interacts with the osteonectin molecule. Through molecular docking analysis between EA and the osteonectin, we identified the specific binding sites on osteonectin for EA that include His232, Tyr263, Glu254, and Lys262 residues. Our findings revealed that EA formed two hydrogen bonds and six hydrophobic bonds with osteonectin, indicating a strong interaction (binding affinity is −6.4 kcal/moL) (Figure 8A–E). These results support the notion that EA could be a promising target for OB differentiation by interacting effectively with osteonectin protein. Furthermore, it is worth noting that osteonectin is acidic and rich in cysteine, which is a crucial noncollagen protein involved in extracellular matrix (ECM) mineralization, influencing various aspects of bone repair and remodeling. Furthermore, osteonectin plays a pivotal role in regulating ECM and collagen synthesis, influencing osteoblast differentiation, maturation, and mineralization, and exhibits a high affinity for type 1 collagen and

https://doi.org/10.1021/acsomega.4c10642
ACS Omega 2025, 10, 15229−15242

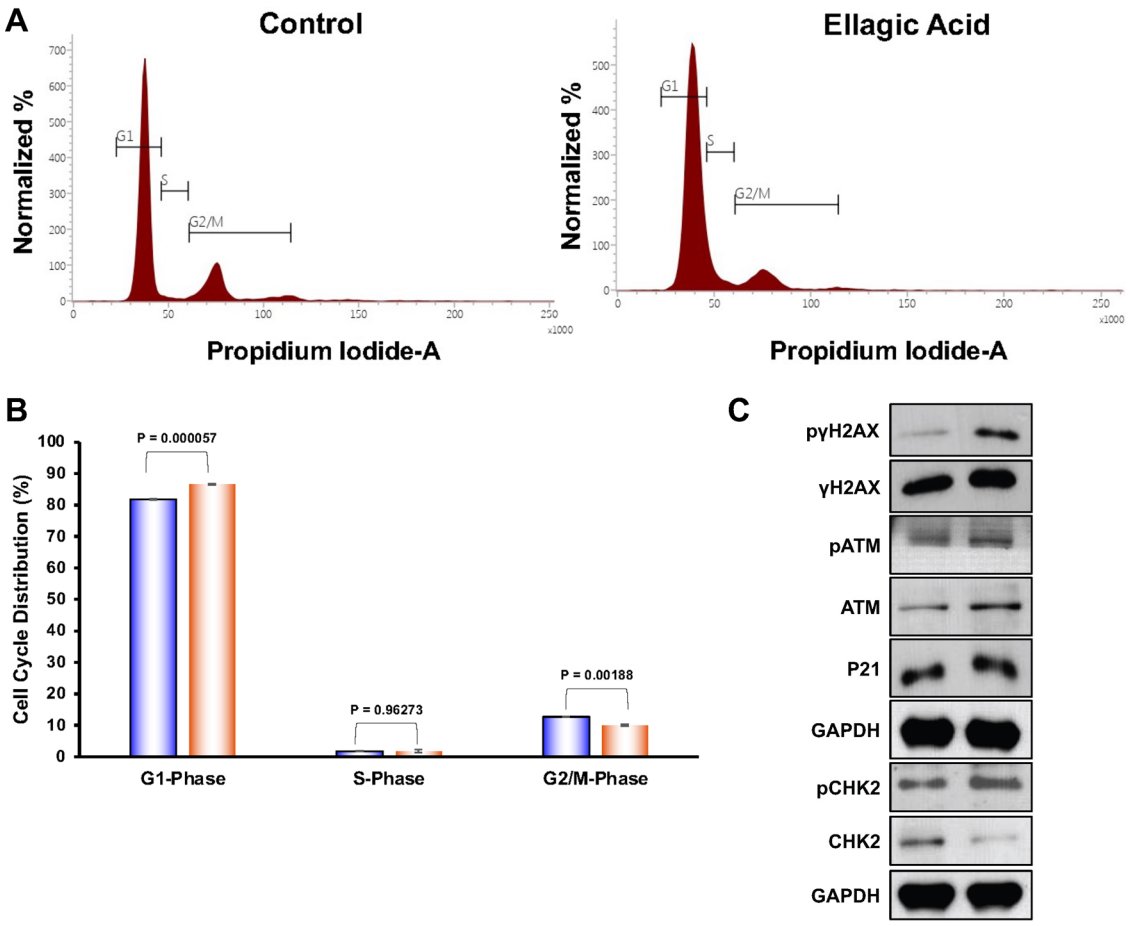

Figure 7. Ellagic acid arrested cell cycle at G1 phase modulating check-point molecules. (A) Cell cycle histograms after 7 days of DPSC in the presence or absence of EA (5 μM). (B) Quantitative graphical representation of percent population in each phase of the cell cycle in the presence or absence of EA (5 μM). (C) The images of Western blot analysis of various check-point molecules (phosphorylated and total).

hydroxylapatite (HA).[34] Western blot confirmed the effect of EA on osteonectin (Figure 8F).

DISCUSSION

The regulation of bone homeostasis is critically important for the maintenance of bone health and is affected by osteoblast and osteoclast differentiation, and dysregulation causes various cartilage and bone-related pathologies. Osteoblasts are responsible for creating the mineral and organic components that make up the skeletal matrix. Both osteopontin (SPP1) and bone sialoprotein (IBSP) are secreted by osteoblasts and affect the nucleation of hydroxyapatite (HA). SPP1 discourages hydroxyapatite formation and encourages OC differentiation, survival, and activity. Conversely, IBSP stimulates hydroxyapatite nucleation.[35] Osteonectin (SPARC) is acidic and rich in the amino acid cysteine, which is a crucial noncollagen protein involved in extracellular matrix (ECM) mineralization, influencing various aspects of bone repair and remodeling. SPARC plays pivotal roles in regulating ECM and collagen synthesis, influencing osteoblast differentiation, maturation, and mineralization, and exhibits a high affinity for type 1 collagen and HA.[34] Even though many treatments are available for pathological conditions like osteoporosis, most of them are only for slowing down the loss of bone density and do not facilitate bone regeneration. So, our study focused on understanding the mechanisms of the effect of EA on DPSC and developing an effective regenerative therapy in the future.

We showed that EA significantly promoted the osteoblastic differentiation of DPSCs by increasing the expression of OB-specific marker molecules including SPARC, BGLAP, SPP1, SP7, and transcription factor RUNX2 both in gene and protein levels. These data are in agreement with the previous findings showing polyphenolic flavonoid compounds induce OB differentiation of MSC or OB precursor cells.[36] Additionally, earlier findings have shown that primary osteoblasts exhibited proliferative activity with EA in a dose-dependent fashion, and the viability of primary osteoblast cells was also notably enhanced.[37] Next, we wanted to know what pathways are involved in EA mediating OB differentiation. BMP2 signaling plays a vital role in osteoblastogenesis throughout the human lifespan. It is indispensable for the formation of new bones during embryogenesis, for the regular formation of bones during the remodeling process of bones, and for the regeneration of bones from any injury.[38] Our results clearly showed that the canonical BMP2 pathways are increased after the addition of EA to the DPSC. BMP2 pathway involves downstream SMAD (Smad 1/5/8 molecules) signaling pathways. Smad proteins are key intermediaries in the BMP and TGF-β signaling pathways, both of which are vital for maintaining bone homeostasis. Reportedly, there are nine Smad members, among which Smad 1, 5, and 8 are key to BMP signaling and are activated by BMPs type I and II or activin receptors 2,[39,40] whereas Smads 2 and 3 specifically mediate the actions of TGF-β or activin.[41] These data are in

https://doi.org/10.1021/acsomega.4c10642
ACS Omega 2025, 10, 15229−15242

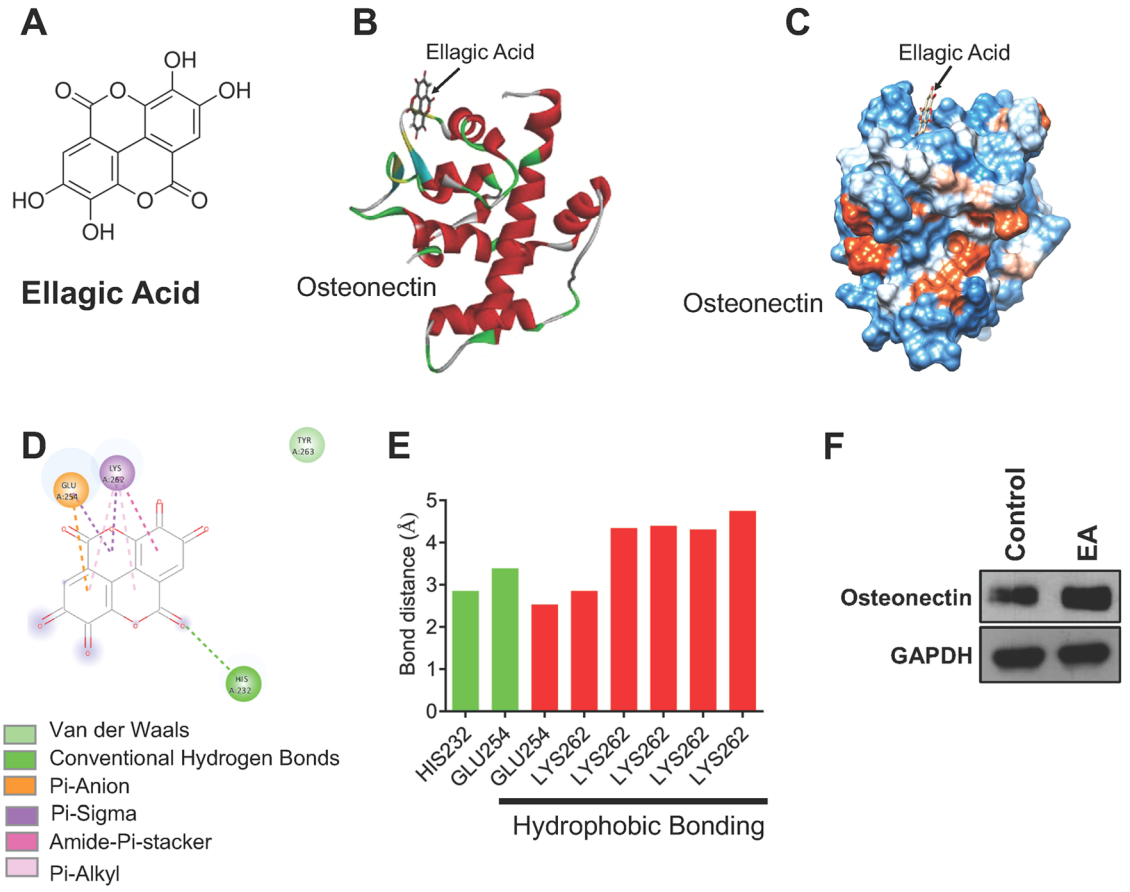

Figure 8. Ellagic acid binding with osteonectin (SPARC). (A) Structure of Ellagic Acid. (B) Docking interaction of ellagic acid with the carboxy-terminal domain of human osteonectin. (C) Docking interaction of ellagic acid with the carboxy-terminal domain of human osteonectin in the gaseous phase. (D) Nonbonding interaction of ellagic acid with human osteonectin. (E) Bond distance between the carboxy-terminal domain of human osteonectin and ellagic acid. (F) Western blot images showing the effect of EA on osteonectin.

agreement with the previous findings showing polyphenolic flavonoid compounds induce OB differentiation of MSC or OB precursor cells using these canonical BMP2 pathways.[42,43] However, interestingly, one of the most studied transcription factors of our lab, KLF2,[6,11,12,27,28,44,45] which plays a critical role in regulating pathogenesis and the cell differentiation process, is also upregulated in both gene and protein levels during the OB differentiation.[11,12,29] The involvement of KLF2 in this OB differentiation process is under investigation and outside of the scope of this manuscript. Osteogenesis is critically dependent on both Wnt and BMP2 signaling involving KLF2 stimulated with a phytoestrogen,[6] and interactions between the two pathways were reported earlier.[25] However, our findings suggest that EA facilitates osteogenesis in DPSCs involving canonical BMP2 pathways. Autophagy plays a significant role in cell survival regulating several essential processes including maintenance of stemness and differentiation, generating cellular energy, and recycling metabolic precursors within the cells. The induction of autophagy helps in developing osteoblast cells and the mineralization process. The number of mitochondria is increased to meet the demand for energy during differentiation.[46] Induction of both autophagy and mitochondria-selective mitophagy can be observed through an increase in the expressions of PINK1 and then parkin.[47] Mitochondria that are damaged initiate the process of mitochondrial fission involving FIS1 and DRP1. We showed an increase in autophagy and mitophagy, which was affirmed by higher levels of autophagic markers such as LC3B, BECN1, ATG3, ATG5, and ATG7; and mitophagy markers PARKIN, DRP1, FIS1, and PINK1 after the addition of EA to the DPSC to induce osteogenesis.

The osteogenic differentiation could be hindered by damage to intracellular organelles and mitochondria caused by excessive reactive oxygen species (ROS).[46] Mitophagy has been found to help clear defective mitochondria and reduce ROS levels in growing cells that are experiencing mild stress conditions, thereby ensuring the survival of the cell.[48] During the OB differentiation, we observed a decrease in the production of intracellular and mitochondrial ROS, which suggests that EA helps to maintain a healthy mitochondrial state by reducing the level of ROS in DPSC. The reduction in mitochondrial membrane potential after the addition of EA was observed after the addition of EA to the DPSC, which is in agreement with the earlier finding suggesting ellagic acid inhibits mitochondrial respiration by altering mitochondrial membrane potential.[49] During OB differentiation, the metabolic reprogramming of stem cells is significantly regulated by mitochondria.[50] It plays a crucial role in regulating various cellular processes, including ROS signaling, calcium signaling, apoptosis, and maintaining cellular homeostasis. Additionally, mitochondria serve as the cell's powerhouse, providing energy during cell differentiation through oxidative phosphorylation.[51,52] Moreover, it directly influences this process by overseeing the cellular redox balance and aiding in the

https://doi.org/10.1021/acsomega.4c10642
ACS Omega 2025, 10, 15229−15242

deposition of the extracellular matrix through processes such as mitophagy, thereby serving as a vital regulator of osteogenesis and the maintenance of bone health.[46] Therefore, it is crucial to comprehend the impact on mitochondrial bioenergetics during the osteogenic differentiation of DPSCs. An improved mitochondrial function may arise from modifications in the dynamic network of mitochondria within cells, adjustments in mitochondrial coupling, or initiation of mitochondrial biogenesis.[53] Differentiated OB-like cells showed an upregulation in mitochondrial respiration and spare respiratory capacity after 7 days indicating that they tend to switch their metabolism toward oxidative phosphorylation, as per previous studies.[53] These studies were consistent with our observations where we found after the addition of EA to the DPSC mitochondrial functions were significantly increased especially in the capacity for glycolysis, glycolytic reserve, nonglycolytic acidification, and glycolysis in differentiated cells in ECAR analysis, and basal respiration, mitochondrial respiration, spare respiration capacity conditions, and ATP production after OCR.

Reactive oxygen species (ROS) can be produced due to metabolic activity, leading to internal DNA damage,[54] and that can lead to the formation of both single- and double-strand breaks and modifications in the base, in turn, activates the signaling pathway of ATM kinase and its downstream events.[55] This process is regulated by an autophosphorylation event that triggers the kinase activity of ATM on downstream targets, such as the histone variant H2AX mainly γ-H2AX.[56] CHK1 and CHK2 are activated upon DNA damage, regulating cell division by controlling different cell cycle proteins. CHK2 can also cause a G1-S arrest and promote P21 expression by phosphorylating P53. These mechanisms prevent damaged DNA transmission to daughter cells and protect cells against pathological conditions.[57] We found that the EA enhances the cell differentiation rate by arresting the cell cycle at the G1/S phase through the activation of the ATM/CHK2 pathway.

In molecular docking, the analysis revealed that EA and osteonectin have strong interactions supporting our hypothesis that EA could be a promising target for OB differentiation. Furthermore, osteonectin is acidic and rich in cysteine, which is crucial for ECM mineralization, influencing various aspects of bone repair and remodeling influencing osteoblast differentiation, maturation, and mineralization, and exhibits a high affinity for type 1 collagen and HA.[34]

Our data establishes that a natural compound EA promotes osteogenic differentiation of DPSC through canonical BMP2 signaling by modulating autophagy, mitophagy pathways, metabolic reprogramming of mitochondrial function, arresting the cell cycle at the G1/S phase through the activation of the ATM/CHK2 pathway, and having strong interaction with osteonectin for ECM mineralization, to influence various aspects of bone repair and remodeling.

METHODS

Reagents. α (α) Modified Essential Medium (MEM, M8042-500 ML), Dulbecco's Modified Eagle Medium (DMEM, D6046-500 ML), Ponceau (P7170), BSA (A9418-100), DCFDA (D6883), and Ellagic Acid (E2250-1G) were procured from Sigma-Aldrich Inc. St. Louis, MO. FBS (Peak Serum, Wellington, CO, #PS-FB3) from Peak Serum, Pen strep (10378-016), Antibiotic-Antimycotic (15240062), L-Glutamine (25030081), Trypsin (25200-056), Cell Dissociation Buffer (13151014), and PBS (70013-032) were procured from Fisher Scientific, Gibco, Waltham, MA. TRIzol reagent (15596018), JC1 dye (T3168), Mitosox red (M36008), Alexa Fluor (A11008), Alexa Fluor (A11001), and mounting medium (P36931) were all acquired from Fisher Scientific, Invitrogen Corporation, Waltham, MA. cDNA kit (4387406), and SYBR Green PCR Kit (4309155) were procured from Applied Biosystem Waltham, MA. Pierce RIPA lysis Buffer (89901), and Super signal west pico plus luminal/enhancer (34578) were acquired from Thermo Fisher Scientific Waltham, MA. TEMED (161-0800) and Bradford reagent (500-0006), Nitrocellulose membrane 0.45 μm (1620115), and Filter paper (1650962) were procured from Bio-Rad, Hercules, CA. Protogel (EC-890) was obtained from National Diagnostics Atlanta, GA. SDS (BP1311-1), DMSO (BP231-100), and Methanol (A412P-4) were all purchased from Fisher Scientific, Hampton, NH. Separating buffer (BP-90), Stacking buffer (BP-95), Running buffer (BP- 150), Transfer buffer (BP-190), and TBST (IBB-180) were all procured from Boston Bioproducts Milford, MA. Nonfat dry milk (M0841) was obtained from LabScientific, Highlands, NJ, and Paraformaldehyde (sc-281692) was procured from Santa Cruz Biotechnology, Dallas, TX. Hanks' balanced salt solution (HBSS, 21-020-CV) was obtained from Mediatech Inc., Manassas, VA, and DEPC-Treated Water (AM9922) was purchased from Thermo Fisher Scientific, Ambion, Waltham, MA. Seahorse XF cell mito-stress kit (103035-100), Glycolysis stress kit (103020-100), XF Base Medium (102353-100), Glucose Solution (103577- 100), Pyruvate Solution (103578−100), Glutamine Solution (103579- 100) and XF calibrant (100840-000) were obtained from Agilent, Santa Clara, CA. Antibodies used for the immunocytochemistry and Western blot (WB) studies are described in Supporting Table S1.

DPSC Isolation and Culture. Human dental pulp-derived stem cells (DPSC) were isolated and cultured according to our lab's previously published protocol.[6] In brief, the DPSC were obtained from the extracted third molar teeth of a healthy adolescent donor with prior IRB approval and donor consent. The teeth were washed thoroughly with PBS containing 1% Antibiotic-Antimycotic solution, at least three times. The pulp was harvested by opening the teeth, minced into 1 mm cubes, plated onto 60 mm cell culture plates, and cultured using αMEM with 20% FBS and 1% Antibiotic-Antimycotic solution. Fresh medium was added every third day following the removal of the old medium. Cells that migrated from the pulp tissues and became confluent were collected by dissociation by cell dissociation buffer and were recultured at passage 1 using the same medium. Cells from passages 2 to 7 were utilized in the experimental procedures.

Osteogenic Differentiation of DPSC. DPSC (passage 2−7) were cultured in 10 cm cell culture dishes in αMEM medium containing 20% FBS (Peak Serum, Wellington, CO, #PS-FB3), 1% anti-anti (Fisher Scientific, Gibco, Waltham, MA, #15240), and 1% α-glutamine (Fisher Scientific, Gibco, Waltham, MA, #25030081). The cells were grown to confluency for 48 h at 37 °C in an incubator with 5% CO_2. To induce OB differentiation, DPSC were trypsinized and seeded into a 12-well plate with DMEM containing 10% FBS, 1% anti-anti, and 1% α-glutamine supplemented with DMSO (vehicle) for the control group, and DMEM supplemented with 5 μM (Total Concentration) EA dissolved in DMSO for the treatment groups. The samples were subsequently put in an incubator and allowed to culture for 7 days while being exposed to 5% CO_2 and maintained at a temperature of 37 °C.

https://doi.org/10.1021/acsomega.4c10642
ACS Omega 2025, 10, 15229−15242

The culture medium was replaced at three-day intervals during this period.

Quantitative RT-PCR. DPSCs were treated with EA for 7 days, and those treated with vehicle were subjected to a TRIzol purification method (Thermo Fisher) to isolate the total RNA. We used the complementary (c) DNA synthesized from the mRNA using the cDNA kit (Thermo Fischer Scientific, Waltham, MA, #4387406), which was used for quantitative PCR using a Bio-Rad CFX96 Real-Time System using SYBR Green PCR (Thermo Fischer Scientific, Waltham, MA, #4309155) for amplification of cDNA. Primers for SPARC (Osteonectin), BGLAP (Osteocalcin), SPP1(Osteopontin), SP7 (Osterix), DXL5, IBSP (Bone sialoprotein), and GAPDH were purchased from Integrated DNA Technologies (Coralville, IA). Sequences are presented in the Supporting Table S2. Cq measurements were obtained, and data are presented as fold difference of ΔΔCT values corrected with GAPDH expression.

Western Blot. Under normal conditions, DPSCs were grown in culture, while the experimental group was exposed to EA (5 μM in DMEM) for 7 days to obtain whole-cell lysates. Protein was quantified by colorimetric assay using the Bradford method (Bio-Rad, Hercules, CA), and the proteins were separated in a polyacrylamide gel. Briefly, a polyacrylamide gel was cast, and denatured proteins (20 μg) were loaded and separated through the gel by electrophoresis; a protein ladder was loaded as a marker (Sigma, St. Louis, MO). The proteins were transferred from the gel to a 0.45 μm nitrocellulose membrane (Bio-Rad) at 4 °C. The blocking of the membrane was carried out at room temperature (RT) for 1 h with a blocking buffer composed of 5% nonfat milk in TBST (TBST) (Boston BioProducts, Ashland, MA). The membrane was first washed three times with TBST and then incubated overnight with a primary antibody against SPARC BGLAP, SPP1, SP7, RUNX2, GAPDH (Cell Signaling, Danvers, MA), and GSK3 (Santa Cruz Biotechnology, Dallas, TX). These primary antibodies were diluted at a ratio of 1:1000 in a solution containing 5% BSA. The membrane underwent washing and was subsequently exposed to a secondary antibody (Cell Signaling, Danvers, MA) diluted to a ratio of 1:3000 and was prepared in a solution consisting of 5% milk in TBST for 2 h. The membrane was then washed, placed in the cassette holder, and incubated briefly in the chemiluminescent substrate (Sigma, St. Louis, MO). Films were then exposed and developed. The densitometrical quantification of the bands was done using the ImageJ software (NIH).

Immunostaining. DPSCs were seeded onto glass coverslips in 6-well plates at a moderate density and cultured in a complete medium containing αMEM, 20% FBS, and 1% PSG, with a volume of 1.5 mL. The next day, the medium was changed to a complete medium containing 5 μM/mL EA or 0.5 μL/mL DMSO in the complete medium as a vehicle-treated control. The medium was removed after 7 days, and the cells were washed with PBS. The cells were subsequently treated by fixing them with 4% paraformaldehyde and permeabilizing them at room temperature (RT) using 1% Triton-X 100. After washing with PBS, cells were blocked in 5% FBS in PBS overnight at 4 °C. Next day; they were washed with wash buffer (PBS with 0.5% FBS and 0.5% TBST) and incubated in primary antibodies for 2 h at RT; two samples were incubated in secondary antibody alone to serve as negative controls. The cell samples were subjected to a washing using a wash buffer. Subsequently, they were exposed to a secondary antibody labeled with a fluorophore (Alexa Fluor 488 α-Rabbit and TX Red α-Goat, depending on the primary antibodies utilized), which had been diluted 1:2000 in wash buffer. The secondary antibody was added to the cells and left to incubate for an hour at room temperature. Glass microscopy slides were used to mount coverslips with ProLong Gold Antifade Mountant containing DAPI (Invitrogen, Carlsbad, CA). Upon drying, fluorescence microscopy was performed, and images were obtained.

Cellular Bioenergetics Analysis. During the osteogenic differentiation of DPSC, the XF 24 Extracellular Flux Analyzer (Seahorse Bioscience in Billerica, MA) was used to assess the mitochondrial respiration, also known as oxygen consumption rate (OCR), and glycolysis, also known as extracellular acidification (ECAR). The process involved dissociating differentiated cells and then reseeding them in a Seahorse Bioscience XF 24-well cell culture microplate in respective media for each condition. The seeding of the cells was performed at a density of (5 × 104) and allowed to grow for 24 h. At the same time, the sensor cartridge of The Seahorse XF calibrant was hydrated overnight in a non-CO2 incubator at 37 °C. The Seahorse analysis was conducted after washing the culture twice with XF base media that was supplemented with pyruvate, glutamine, and glucose to ensure optimal conditions for the study. Next, 500 μL of the medium/well was added to all the wells. Then, plates were incubated in a non-CO2 incubator at 37 °C for 1 h. After that, Seahorse XF calibrant was supplemented with the ATP synthase inhibitor, oligomycin (1.5 μM), uncoupler carbonyl cyanide-4-(trifluoromethoxy) phenylhydrazone (FCCP, 1 μM), complex III inhibitor rotenone, and antimycin A (0.5 μM) and then first calibrated the instrument using Seahorse Wave software 2.6.1. After replacing the calibrant plate, the XF 24-well cell culture microplate was utilized for the OCR measurement. The measurement was done in terms of ATP turnover, maximal respiration, and reserve respiratory capacity. The glycolysis stress test was carried out by administering glucose (1 mM), oligomycin (1 μM), and 2-deoxyglucose (10 mM) sequentially. ECAR parameters were calculated using Seahorse Wave software 2.6.1.

Cellular ROS Analysis. To analyze the production of Reactive Oxygen Species (ROS) within the cells, a compound called DCFDA (Sigma-Aldrich, St. Louis, MO) was used. DCFDA is a compound known as 2′,7′-dichlorodihydrofluorescein diacetate. Intracellular ROS reacts with nonfluorescent DCFDA and converts it into fluorescent molecules. In brief, DPSC (8×10^4) were seeded on a six-well plate overnight. Next, the medium was substituted with a medium containing EA and incubated for 7 days. After incubation, cells were rinsed with 1× PBS, and then exposed to a 5 μM DCFDA working solution, which was prepared in 1× PBS, for 20 min at 37 °C. Following washing with 1× PBS, the images of cells were captured and analyzed using a Leica Stellaris 8 Falcon STED confocal microscope, with the excitation set at 495 nm and the emission at 529 nm.

Mitochondrial ROS Analysis. Cellular generation of reactive oxygen species (ROS) in mitochondria was estimated by utilizing the MitoSOX red compound (Thermo Scientific, Waltham, MA). MitoSOX red is a nonfluorescent dye that gets oxidized with free radicals produced by mitochondrial superoxide, leading to the production of red fluorescence.

To carry out the experiment, DPSC (8×10^4) were seeded on a six-well plate overnight. The next day, the medium was

https://doi.org/10.1021/acsomega.4c10642
ACS Omega 2025, 10, 15229−15242

replaced with EA and incubated for 7 days. Using 1× PBS, the cells were washed following the incubation period and then treated with a working solution consisting of 5 μM MitoSOX red in Hanks' balanced salt solution (HBSS). The exposure lasted for 15 min at 37 °C. Following the exposure, the cells were washed with 1× PBS, and their images were captured and analyzed using a Leica Stellaris 8 Falcon STED confocal microscope with the setting of excitation and emission at 510/588 nm.

Molecular Docking. Molecular docking is a multistep process crucial for predicting molecular interactions. Initially, EA's structure underwent optimization using Gaussian 09 software at the semiempirical PM6 level in the gas phase. The SPARC domain's crystal structure (PDB ID: 1SRA) was retrieved from the protein data bank (PDB). Following consideration of the entire protein sequence, water atoms were removed via PyMOL Molecular Graphics System software. Protein structure optimization for minimum energy ensued with the Swiss-PDB viewer software. Subsequently, Autodock Vina software facilitated the computation of nonbonding interactions and binding affinities between the ligand and protein. Finally, analysis of nonbonding interactions with respective proteins was carried out using PyMOL Molecular Graphics System and Discovery Studio.

Statistical Analysis. The experiments were repeated at least three times in a triplicate manner, and the findings were expressed as mean ± SEM. The statistical analysis was carried out using the Graph Pad Prism 5.0 software (Graph Pad Software, San Diego, CA). The software used to perform statistical analysis of the experimental results was conducted using a two-tailed Student's t test, and p values less than 0.05 were considered significant, and the exact p values were provided in the graphs.

■ ASSOCIATED CONTENT

Data Availability Statement

Data supporting the study are available in the published article and its Supporting Information.

Supporting Information

The Supporting Information is available free of charge at https://pubs.acs.org/doi/10.1021/acsomega.4c10642.

Figure S1. Bar graphs show the quantified level of osteonectin (SPARC), osteocalcin (BGLAP), osteopontin (SPP1), osterix (SP7), and RUNX2 protein compared to the GAPDH level shown in Figure 1C; Figure S2. Bar graphs show the quantified amount of BMP2/4, SMAD1/5/8, and KLF2, protein levels compared to the GAPDH level shown in Figure 2C; Figure S3. Bar graphs show the quantified level of autophagy molecules including LC3B, ATG7, ATG3, and Beclin1 levels compared to the GAPDH level shown in Figure 3C; Figure S4. Bar graphs show the quantified level of mitophagy marker proteins including PARKIN, DRP1, FIS1, and PINK1 levels compared to the GAPDH level shown in Figure 4C; Figure S5. (A) Showing original Seahorse flux analysis graph of extracellular acidification rate (ECAR) after 7 days of DPSC in the presence or absence of EA (5 μM). (B) Showing original seahorse flux analysis graph of oxygen consumption rate (OCR) after 7 days of DPSC in the presence or absence of EA (5 μM); Figure S6. Bar graphs show the quantified levels of check-point proteins including pγH2AX, γH2AX, pATM, ATM, P21, pCHK2, and CHK2 levels compared to the GAPDH level shown in Figure 8C; Figure S7. The bar graph shows the quantified level of osteonectin (SPARC) compared to the GAPDH level shown in Figure 8F; Table S1. Details of antibodies used in this study; Table S2. Primer sequences of genes used in quantitative RT-PCR experiments (PDF)

■ AUTHOR INFORMATION

Corresponding Author

Hiranmoy Das − *Department of Pharmaceutical Sciences, Jerry H. Hodge School of Pharmacy, Texas Tech University Health Sciences Center, Amarillo, Texas 79106, United States;* orcid.org/0000-0002-3343-0096; Phone: 8064149623; Email: hiranmoy.das@ttuhsc.edu; Fax: 8063564770

Authors

Prathyusha Naidu − *Department of Pharmaceutical Sciences, Jerry H. Hodge School of Pharmacy, Texas Tech University Health Sciences Center, Amarillo, Texas 79106, United States*

Manjusri Das − *Department of Pharmaceutical Sciences, Jerry H. Hodge School of Pharmacy, Texas Tech University Health Sciences Center, Amarillo, Texas 79106, United States*

Surajit Hansda − *Department of Pharmaceutical Sciences, Jerry H. Hodge School of Pharmacy, Texas Tech University Health Sciences Center, Amarillo, Texas 79106, United States*

Prateeksha Prateeksha − *Department of Pharmaceutical Sciences, Jerry H. Hodge School of Pharmacy, Texas Tech University Health Sciences Center, Amarillo, Texas 79106, United States*

Md Sariful Islam Howlader − *Department of Pharmaceutical Sciences, Jerry H. Hodge School of Pharmacy, Texas Tech University Health Sciences Center, Amarillo, Texas 79106, United States*

Md Afjalus Siraj − *Department of Therapeutic Radiology, Yale School of Medicine, Yale University, New Haven, Connecticut 06520, United States*

Complete contact information is available at: https://pubs.acs.org/10.1021/acsomega.4c10642

Author Contributions

All authors were involved in drafting the article or revising it critically for important intellectual content, and all authors approved the final version to be published. Study conception, design, and manuscript writing: P.N. and H.D. Acquisition of data: P.N., M.S.I.H., M.D., S.H., P.P., M.A.S. Analysis and interpretation of data: P.N. and H.D.

Funding

This work was supported in part by National Institutes of Health grants, R01AR068279 (NIAMS), STTR R42EY031196 (NEI), and STTR 1R41AG057242 (NIA). The funders had no role in the study design, data collection, and analysis, decision to publish, or preparation of the manuscript.

Notes

The authors declare no competing financial interest.
Authors provide the consent for publication.
AI in scientific writing The authors did not use any AI-assisted technologies in the manuscript writing process.

■ ACKNOWLEDGMENTS

Authors are thankful to Zijuan Liu, from the TTUHSC core facility for her help in procuring some of the confocal images. The core facility is being supported by a Core Facility Support Award (grant number RP200572) from the Cancer Prevention and Research Institute of Texas (CPRIT) to the Imaging Core, Texas Tech University Health Sciences Center at Amarillo.

■ REFERENCES

(1) Ríos, J.-L.; Giner, R. M.; Marín, M.; Recio, M. C. A pharmacological update of ellagic acid. *Planta Med.* **2018**, *84* (15), 1068−1093.
(2) Rantlha, M.; Sagar, T.; Kruger, M. C.; Coetzee, M.; Deepak, V. Ellagic acid inhibits RANKL-induced osteoclast differentiation by suppressing the p38 MAP kinase pathway. *Arch. Pharmacal Res.* **2017**, *40*, 79−87.
(3) Lin, X.; Yuan, G.; Li, Z.; Zhou, M.; Hu, X.; Song, F.; et al. Ellagic acid protects ovariectomy-induced bone loss in mice by inhibiting osteoclast differentiation and bone resorption. *J. Cell. Physiol.* **2020**, *235* (9), 5951−5961.
(4) Wardhana, A. S.; Nirwana, I.; Budi, H. S.; Surboyo, M. D. C. Role of hydroxyapatite and ellagic acid in the osteogenesis. *Eur. J. Dent.* **2021**, *15* (01), 008−012.
(5) Wang, J.; Zhang, Y.; Cao, J.; Wang, Y.; Anwar, N.; Zhang, Z.; et al. The role of autophagy in bone metabolism and clinical significance. *Autophagy* **2023**, *19* (9), 2409−2427.
(6) Rolph, D. N.; Deb, M.; Kanji, S.; Greene, C. J.; Das, M.; Joseph, M.; et al. Ferutinin directs dental pulp-derived stem cells towards the osteogenic lineage by epigenetically regulating canonical Wnt signaling. *Biochim. Biophys. Acta, Mol. Basis Dis.* **2020**, *1866* (4), No. 165314.
(7) Lu, S.-Y.; Wang, C.-Y.; Jin, Y.; Meng, Q.; Liu, Q.; Liu, Z.-h.; et al. The osteogenesis-promoting effects of alpha-lipoic acid against glucocorticoid-induced osteoporosis through the NOX4, NF-kappaB, JNK and PI3K/AKT pathways. *Sci. Rep.* **2017**, *7* (1), No. 3331.
(8) Lademann, F.; Hofbauer, L. C.; Rauner, M. The bone morphogenetic protein pathway: the osteoclastic perspective. *Front. Cell Develop. Biol.* **2020**, *8*, No. 586031.
(9) Marzona, L.; Pavolini, B. Play and players in bone fracture healing match. *Clin Cases Miner. Bone Metab.* **2009**, *6* (2), 159−162.
(10) Knight, M. N.; Hankenson, K. D. Mesenchymal stem cells in bone regeneration. *Adv. Wound Care* **2013**, *2* (6), 306−316.
(11) Prateeksha, P.; Naidu, P.; Das, M.; Barthels, D.; Das, H. KLF2 Regulates Neural Differentiation of Dental Pulp-derived Stem Cells by Modulating Autophagy and Mitophagy. *Stem Cell Rev. Rep.* **2023**, *19* (8), 2886−2900.
(12) Hansda, S.; Prateeksha, P.; Das, H. Krüppel-like factor 2 (KLF2), a potential target for neuroregeneration. *Neural Regener. Res.* **2024**, *19* (11), 2327−2328.
(13) Gronthos, S.; Mankani, M.; Brahim, J.; Robey, P. G.; Shi, S. Postnatal human dental pulp stem cells (DPSCs) in vitro and in vivo. *Proc. Natl. Acad. Sci.* **2000**, *97* (25), 13625−13630.
(14) Paino, F.; La Noce, M.; Giuliani, A.; De Rosa, A.; Mazzoni, S.; Laino, L.; et al. Human DPSCs fabricate vascularized woven bone tissue: a new tool in bone tissue engineering. *Clin. Sci.* **2017**, *131* (8), 699−713.
(15) Halloran, D.; Durbano, H. W.; Nohe, A. Bone morphogenetic protein-2 in development and bone homeostasis. *J. Dev. Biol.* **2020**, *8* (3), No. 19.
(16) Cejalvo, T.; Sacedón, R.; Hernández-López, C.; Diez, B.; Gutierrez-Frías, C.; Valencia, J.; et al. Bone morphogenetic protein-2/4 signalling pathway components are expressed in the human thymus and inhibit early T-cell development. *Immunology* **2007**, *121* (1), 94−104.
(17) Liu, D.-B.; Sui, C.; Wu, T.-T.; Wu, L.-Z.; Zhu, Y.-Y.; Ren, Z.-H. Association of bone morphogenetic protein (BMP)/Smad signaling pathway with fracture healing and osteogenic ability in senile osteoporotic fracture in humans and rats. *Med. Sci. Monit.* **2018**, *24*, 4363.
(18) Zhao, B.; Xing, G.; Wang, A. The BMP signaling pathway enhances the osteoblastic differentiation of bone marrow mesenchymal stem cells in rats with osteoporosis. *J. Orthop. Surg. Res.* **2019**, *14*, No. 462.
(19) Wu, M.; Chen, G.; Li, Y.-P. TGF-β and BMP signaling in osteoblast, skeletal development, and bone formation, homeostasis and disease. *Bone Res.* **2016**, *4* (1), 1−21.
(20) Asadi, A.; Goudarzi, F.; Ghanadian, M.; Mohammadalipour, A. Evaluation of the osteogenic effect of apigenin on human mesenchymal stem cells by inhibiting inflammation through modulation of NF-κB/IκBα. *Res. Pharm. Sci.* **2022**, *17* (6), 697−706.
(21) Jolette, J.; Attalla, B.; Varela, A.; Long, G. G.; Mellal, N.; Trimm, S.; et al. Comparing the incidence of bone tumors in rats chronically exposed to the selective PTH type 1 receptor agonist abaloparatide or PTH (1−34). *Regul. Toxicol. Pharmacol.* **2017**, *86*, 356−365.
(22) Goto, T.; Hagiwara, K.; Shirai, N.; Yoshida, K.; Hagiwara, H. Apigenin inhibits osteoblastogenesis and osteoclastogenesis and prevents bone loss in ovariectomized mice. *Cytotechnology* **2015**, *67*, 357−365.
(23) Papapetrou, P. D. Bisphosphonate-associated adverse events. *Hormones* **2009**, *8* (2), 96−110.
(24) Gong, L.; Altman, R. B.; Klein, T. E. Bisphosphonates pathway. *Pharmacogenet. Genomics* **2011**, *21* (1), 50−53.
(25) Maity, J.; Barthels, D.; Sarkar, J.; Prateeksha, P.; Deb, M.; Rolph, D.; Das, H. Ferutinin induces osteoblast differentiation of DPSCs via induction of KLF2 and autophagy/mitophagy. *Cell Death Dis.* **2022**, *13* (5), 452.
(26) Greene, C. J.; Anderson, S.; Barthels, D.; Howlader, M. S. I.; Kanji, S.; Sarkar, J.; Das, H. DPSC Products Accelerate Wound Healing in Diabetic Mice through Induction of SMAD Molecules. *Cells* **2022**, *11* (15), No. 2409.
(27) Das, H.; Kumar, A.; Lin, Z.; Patino, W. D.; Hwang, P. M.; Feinberg, M. W.; et al. Kruppel-like factor 2 (KLF2) regulates proinflammatory activation of monocytes. *Proc. Natl. Acad. Sci. U.S.A.* **2006**, *103* (17), 6653−6658.
(28) Laha, D.; Deb, M.; Das, H. KLF2 (kruppel-like factor 2 [lung]) regulates osteoclastogenesis by modulating autophagy. *Autophagy* **2019**, *15* (12), 2063−2075.
(29) Maity, J.; Deb, M.; Greene, C.; Das, H. KLF2 regulates dental pulp-derived stem cell differentiation through the induction of mitophagy and altering mitochondrial metabolism. *Redox Biol.* **2020**, *36*, No. 101622.
(30) Rolph, D.; Das, H. Transcriptional regulation of osteoclastogenesis: the emerging role of KLF2. *Front. Immunol.* **2020**, *11*, No. 937.
(31) Sarkar, J.; Das, M.; Howlader, M. S. I.; Prateeksha, P.; Barthels, D.; Das, H. Epigallocatechin-3-gallate inhibits osteoclastic differentiation by modulating mitophagy and mitochondrial functions. *Cell Death Dis.* **2022**, *13* (10), 908.
(32) Laha, D.; Sarkar, J.; Maity, J.; Pramanik, A.; Howlader, M. S. I.; Barthels, D.; Das, H. Polyphenolic Compounds Inhibit Osteoclast Differentiation While Reducing Autophagy through Limiting ROS and the Mitochondrial Membrane Potential. *Biomolecules* **2022**, *12* (9), No. 1220, DOI: 10.3390/biom12091220.
(33) Akaike, T.; Ida, T.; Wei, F.-Y.; Nishida, M.; Kumagai, Y.; Alam, M. M.; et al. Cysteinyl-tRNA synthetase governs cysteine polysulfidation and mitochondrial bioenergetics. *Nat. Commun.* **2017**, *8* (1), No. 1177.
(34) Zhu, Y. S.; Mo, T. T.; Jiang, C.; Zhang, J. N. Osteonectin bidirectionally regulates osteoblast mineralization. *J. Orthop. Surg. Res.* **2023**, *18* (1), No. 761.
(35) Luukkonen, J.; Hilli, M.; Nakamura, M.; Ritamo, I.; Valmu, L.; Kauppinen, K.; et al. Osteoclasts secrete osteopontin into resorption lacunae during bone resorption. *Histochem. Cell Biol.* **2019**, *151*, 475−487.

(36) Liu, H.; Yi, X.; Tu, S.; Cheng, C.; Luo, J. Kaempferol promotes BMSC osteogenic differentiation and improves osteoporosis by downregulating miR-10a-3p and upregulating CXCL12. *Mol. Cell. Endocrinol.* **2021**, *520*, No. 111074.
(37) Guo, L.; Wei, P.; Li, S.; Zhou, L.; Yan, Y.; Li, D. Ellagic acid prevents ovariectomy-induced bone loss and attenuates oxidative damage of osteoblasts by activating SIRT1. *J. Nat. Med.* **2024**, *79*, 371−380.
(38) Rosen, V. BMP2 signaling in bone development and repair. *Cytokine Growth Factor Rev.* **2009**, *20* (5−6), 475−480.
(39) Derynck, R.; Zhang, Y. E. Smad-dependent and Smad-independent pathways in TGF-β family signalling. *Nature* **2003**, *425* (6958), 577−584.
(40) Gomez-Puerto, M. C.; Iyengar, P. V.; García de Vinuesa, A.; Ten Dijke, P.; Sanchez-Duffhues, G. Bone morphogenetic protein receptor signal transduction in human disease. *J. Pathol.* **2019**, *247* (1), 9−20.
(41) Zou, M.-L.; Chen, Z.-H.; Teng, Y.-Y.; Liu, S.-Y.; Jia, Y.; Zhang, K.-W.; et al. The Smad dependent TGF-β and BMP signaling pathway in bone remodeling and therapies. *Front. Mol. Biosci.* **2021**, *8*, No. 593310.
(42) Sharifi, S.; Moghaddam, F. A.; Abedi, A.; Dizaj, S. M.; Ahmadian, S.; Abdolahinia, E. D.; et al. Phytochemicals impact on osteogenic differentiation of mesenchymal stem cells. *Biofactors* **2020**, *46* (6), 874−893.
(43) Zhang, J. L.; Liu, Z. H.; Luo, Y.; Li, X. J.; Huang, G. W.; Chen, H.; et al. The Role of Flavonoids in the Osteogenic Differentiation of Mesenchymal Stem Cells. *Front. Pharmacol.* **2022**, *13*, No. 849513, DOI: 10.3389/fphar.2022.849513.
(44) Das, M.; Deb, M.; Laha, D.; Joseph, M.; Kanji, S.; Aggarwal, R.; et al. Myeloid Kruppel-Like Factor 2 Critically Regulates K/BxN Serum-Induced Arthritis. *Cells* **2019**, *8* (8), No. 908, DOI: 10.3390/cells8080908.
(45) Jha, P.; Das, H. KLF2 in regulation of NF-κB-mediated immune cell function and inflammation. *Int. J. Mol. Sci.* **2017**, *18* (11), No. 2383.
(46) Gao, J.; Feng, Z.; Wang, X.; Zeng, M.; Liu, J.; Han, S.; et al. SIRT3/SOD2 maintains osteoblast differentiation and bone formation by regulating mitochondrial stress. *Cell Death Differ.* **2018**, *25* (2), 229−240.
(47) Jin, S. M.; Lazarou, M.; Wang, C.; Kane, L. A.; Narendra, D. P.; Youle, R. J. Mitochondrial membrane potential regulates PINK1 import and proteolytic destabilization by PARL. *J. Cell Biol.* **2010**, *191* (5), 933−942.
(48) Zhang, J. Autophagy and mitophagy in cellular damage control. *Redox Biol.* **2013**, *1* (1), 19−23.
(49) Duan, J.; Li, Y.; Gao, H.; Yang, D.; He, X.; Fang, Y.; Zhou, G. Phenolic compound ellagic acid inhibits mitochondrial respiration and tumor growth in lung cancer. *Food Funct.* **2020**, *11* (7), 6332−6339.
(50) Riddle, R. C.; Clemens, T. L. Bone cell bioenergetics and skeletal energy homeostasis. *Physiol. Rev.* **2017**, *97* (2), 667−698.
(51) Kuntz, E. M.; Baquero, P.; Michie, A. M.; Dunn, K.; Tardito, S.; Holyoake, T. L.; et al. Targeting mitochondrial oxidative phosphorylation eradicates therapy-resistant chronic myeloid leukemia stem cells. *Nat. Med.* **2017**, *23* (10), 1234−1240.
(52) Shares, B. H.; Busch, M.; White, N.; Shum, L.; Eliseev, R. A. Active mitochondria support osteogenic differentiation by stimulating β-catenin acetylation. *J. Biol. Chem.* **2018**, *293* (41), 16019−16027.
(53) Smith, C. O.; Eliseev, R. A. Energy metabolism during osteogenic differentiation: the role of Akt. *Stem Cells Dev.* **2021**, *30* (3), 149−162.
(54) Sjakste, N.; Riekstiņa, U. DNA damage and repair in the differentiation of stem cells and cells of connective cell lineages: A trigger or a complication? *Eur. J. Histochem.* **2021**, *65* (2), No. 3236, DOI: 10.4081/ejh.2021.3236.
(55) Lu, J.; Das, M.; Kanji, S.; Aggarwal, R.; Joseph, M.; Ray, A.; et al. Induction of ATM/ATR pathway combined with Vγ2Vδ2 T cells enhances cytotoxicity of ovarian cancer cells. *Biochim. Biophys. Acta, Mol. Basis Dis.* **2014**, *1842* (7), 1071−1079.
(56) Rosina, M.; Langone, F.; Giuliani, G.; Cerquone Perpetuini, A.; Reggio, A.; Calderone, A.; et al. Osteogenic differentiation of skeletal muscle progenitor cells is activated by the DNA damage response. *Sci. Rep.* **2019**, *9* (1), No. 5447.
(57) van Jaarsveld, M. T. M.; Deng, D.; Ordoñez-Rueda, D.; Paulsen, M.; Wiemer, E. A.; Zi, Z. Cell-type-specific role of CHK2 in mediating DNA damage-induced G2 cell cycle arrest. *Oncogenesis* **2020**, *9* (3), No. 35.

https://doi.org/10.1021/acsomega.4c10642
ACS Omega 2025, 10, 15229−15242